

**TUNABLE DRUG LOADING AND REINFORCEMENT OF  
POLYCAPROLACTONE FILMS BY MEANS OF  
ELECTROSPUN NANOFIBERS OF GLYCOLIDE  
SEGMENTED COPOLYMERS**

**Yolanda Márquez<sup>1,2</sup>, Lourdes Franco<sup>1</sup>, Pau Turon<sup>2</sup>,  
Luís J. del Valle<sup>1</sup>, Jordi Puiggali<sup>1\*</sup>**

*<sup>1</sup>Departament d'Enginyeria Química, Universitat Politècnica de Catalunya, Av.  
Diagonal 647, Barcelona E-08028, SPAIN*

*<sup>2</sup>B. Braun Surgical S.A., Carretera de Terrasa 121, Rubí (Barcelona), 08191, SPAIN*

*Correspondence to: J. Puiggali (Phone: 34-934015649, E-mail: [Jordi.Puiggali@upc.edu](mailto:Jordi.Puiggali@upc.edu))*

## ABSTRACT

Electrospinning of a segmented copolymer having polyglycolide hard segments was successfully performed from 1,1,1,3,3,3-hexafluoroisopropanol solutions. During the process, a bactericidal agent, i.e. chlorhexidine (CHX), was effectively loaded, which resulted in nanofibers with a smaller diameter because of the change in solution conductivity. New fabrics based on molding of alternate layers of poly( $\epsilon$ -caprolactone) (PCL) films and the electrospun scaffolds of the segmented copolymer were prepared and characterized. The thermal molding process rendered a PCL matrix homogeneously reinforced with nanofibers that compensated for the loss of mechanical properties caused by incorporation of CHX.

Release of CHX was evaluated in different media. Results varied depending on the layer where the drug was incorporated. Thus, systems with an immediate bacteriostatic effect, as well as systems with a potential long term antimicrobial effect, were obtained. Growth inhibition and adhesion assays demonstrated the fast bactericidal effect of samples with CHX loaded in its outer layers.

**Keywords:** Biocompatibility, biodegradable, block copolymers, poly( $\epsilon$ -caprolactone), polyesters, drug delivery systems, reinforcement, mechanical properties.

## INTRODUCTION

Electrospun nanofibers **have great potential** as reinforcing materials due to their anisotropy and high surface/volume ratio. They can also be used for encapsulation of drugs due to their high drug loading capability as provided by the electrospinning process. **The mechanical properties of polymer matrices are generally affected by the addition of drugs. This can be counteracted by using suitable reinforcing agents. Furthermore, drug release can be tuned by appropriate choice of nanofiber composition and of drug loading area** (e.g. slow and fast releases should be expected when drugs are incorporated in the matrix or the filler, respectively). Several recent works focus on the use of electrospun micro/nanofibers as fillers and demonstrate the improvement of mechanical properties of derived composites [1-5]. In this sense, good distribution of fibers and absence of interleaves are significant factors that must be taken into account [5].

Drug release behavior can be modified by varying the composition of the encapsulating system. For example, tuned release of a model drug such as triclosan can be achieved by employing electrospun fibers prepared from different mixtures of polylactide and poly( $\epsilon$ -caprolactone) [6]. A similar effect can be attained from copolymers with different compositions, among which poly(lactic acid-*co*-glycolic acid) (PLGA) is probably the most widely studied. **It is also** worth considering the use of segmented copolymers because they could provide better properties than the above random copolymers. Furthermore, it seems possible to have control over the final mechanical performance by changing the ratio between the stiff hard blocks and flexible soft blocks which characterize the segmented architecture [7].

Poly( $\epsilon$ -caprolactone) (PCL) is a biodegradable, **biocompatible, easily processed polymer. Despite significant** disadvantages such as poor barrier properties, low melting

temperature and low modulus, PCL has wide applications in tissue engineering, drug delivery and packaging [8-10]. Therefore, PCL appears as an ideal matrix for successful loading of biodegradable, biocompatible nanofillers which improve its mechanical properties and extend its range of application as a drug delivery system.

Although electrospun fibers of polyglycolide (PGL) seem good fillers due to their relatively high degradation rate and high tensile modulus, it should be considered that PGL has a highly hydrophilic character, which contrasts with the hydrophobicity of PCL. A lack of surface adhesion between PCL and PGL homopolymers **resulting in limited benefits in terms of mechanical properties is expected**. The use of electrospun fibers from PCL and PGL mixtures has been considered a good alternative to improve adhesion and make load transfer from the PCL matrix to the stronger fiber reinforcement feasible [11]. Specifically, it was determined that incorporation of 40 wt-% of fibers constituted by equivalent **percentages** of PCL and PGL led to increased yield strength.

**The present work aims** to evaluate the use of segmented polymers incorporating compatible  $\epsilon$ -caprolactone units as reinforcing materials. Poly(GL)-*b*-poly(GL-*co*-TMC-*co*-CL)-*b*-poly(GL) (Figure 1a) was selected because it is a commercial bioabsorbable suture (Monosyn<sup>®</sup>) with high crystallinity, good mechanical properties and high biodegradability [12-15]. **Monosyn<sup>®</sup> is constituted by two polyglycolide hard segments and a relatively hydrophobic soft segment that corresponds to a weight of 43%. The middle soft segment is characterized by a random distribution of  $\epsilon$ -caprolactone residues (32.5 wt-%), together with glycolide (35 wt-%) and trimethylene carbonate (32.5 wt-%) units [16].**

Electrospinning of PGL copolymers having a segmented architecture has not been undertaken up to now. Even electrospinning of polyglycolide has scarcely been

addressed despite its wide application in the biomedical field. Nevertheless, it has been reported that PGL electrospun nanofibers can be prepared from 8 wt-% in HFIP solution, with an average fiber diameter of 310 nm and a diameter distribution between 50 and 650 nm [17].

A multilayer system is a new approach to obtain reinforced matrices. The use of different layers combining polymeric films and electrospun scaffolds allows mechanical properties and even drug release to be tailored by appropriate selection of the layer where the pharmacological agent is incorporated.

The present work focuses on a system formed by five layers, three of poly( $\epsilon$ -caprolactone) films and two of electrospun poly(GL)-*b*-poly(GL-*co*-TMC-*co*-LA)-*b*-poly(GL) mats (Figure 1b). The use of this kind of systems for controlling drug release is evaluated using a hydrophilic drug such as CHX (1,1'-hexamethylene-bis-5-(4-chlorophenyl)biguanide) (Figure 1a). This drug is very interesting due to its high antimicrobial activity [18]. Specifically, protonated secondary amines of CHX can be attached to negatively loaded (anionic) phospholipids of the bacterial membranes [19], causing the destabilization of the cell wall and interfering with osmosis. It is expected that CHX can be quickly delivered from a hydrophobic matrix into a hydrophilic medium. For this reason, it is a good model to evaluate loading capability from different configurations to achieve delayed release.

## EXPERIMENTAL SECTION

### Materials

Commercially available violet sutures of poly(GL)-*b*-poly(GL-*co*-TMC-*co*-CL)-*b*-poly(GL) (Monosyn<sup>®</sup>, USP 0) with a weight average molecular weight of 90,700 g/mol were kindly supplied by B. Braun Surgical, S.A. Poly( $\epsilon$ -caprolactone) (PCL) ( $M_w$ :

65000 g/mol), chlorhexidine diacetate (CHX) and phosphate buffered saline (PBS - Dulbecco's Phosphate Buffer Saline) were purchased from Sigma-Aldrich.

Ethanol absolute and methanol were purchased from Scharlab and 1,1,1,3,3,3-hexafluoroisopropanol (HFIP) from Apollo Scientific.

Reagents and labware for microbial culture were also obtained from Scharlab. The bacterial strains *Escherichia coli* CECT 101 and *Staphylococcus aureus* CECT 245 were obtained from the Spanish Type Culture Collection (Valencia, Spain).

## **Measurements**

Tensile properties of 1 cm x 2 cm samples of PCL films, electrospun mats and the resulting matrices were studied at room temperature and humidity using a universal tensile testing instrument Zwick Z2.5/TN1S with a 100 N load cell equipped with a testXpert 8.1 program. Thickness of specimens depended on the preparation method. Specifically, values of 0.2, 0.05 and 0.7 mm were determined for films, electrospun mats and melt pressed matrices, respectively. Initial distance between clamps was 10 mm and crosshead speed was 10 mm/min. The reported Young's modulus and tensile strength were averaged values of at least five specimens.

Scanning electron microscopy (SEM) was employed to examine the morphology of electrospun fibers and fracture surfaces. Carbon coating was accomplished with a Mitec k950 Sputter Coater (fitted with a film thickness monitor k150x (Quorum Technologies Ltd., West Sussex, UK). SEM micrographs were taken with a Zeiss Neon 40 EsB instrument (Carl Zeiss, Oberkochen, Germany).

Calorimetric data were obtained by differential scanning calorimetry with a TA Instruments Q100 series with  $T_{zero}$  technology and equipped with a refrigerated cooling system (RCS). Experiments were conducted under a flow of dry nitrogen at a heating

rate of 20 °C/min with a sample weight of approximately 5 mg. Calibration was performed with indium.

Thermal degradation was determined at a heating rate of 10 °C/min with around 5 mg of samples in a Q50 thermogravimetric analyzer of TA Instruments under a flow of dry nitrogen and in the temperature range from 50 to 600 °C.

### **Electrospinning of poly(GL)-*b*-poly(GL-co-TMC-co-CL)-*b*-poly(GL)**

Electrospinning of poly(GL)-*b*-poly(GL-co-TMC-co-CL)-*b*-poly(GL) was carried out in HFIP with a polymer concentration of 10 w/v-%. CHX loaded samples were obtained by adding 0.5 w/w-% of the drug in the electrospinning solution.

Electrospun fibers were collected on a rotating grounded collector operating at 30 rpm and at a variable distance (10-15 cm) at room temperature. The voltage was varied between 10 and 30 kV and applied to the collector using a high-voltage supplier (Gamma High Voltage Research, ES30-5W). The polymer solution was delivered via a KDS100 infusion syringe pump (KD Scientific, USA) to control the flow rate (from 3.5 to 10 mL h<sup>-1</sup>).

Unloaded and CHX loaded electrospun fibers were prepared using optimized parameters (i.e. needle-collector distance, voltage and flow rates) and solvent conditions (i.e. specific solvent and polymer concentration).

### **Preparation of loaded and unloaded PCL films**

PCL films were prepared by pressing 0.7 g of PCL in a 4 cm x 6 cm flat mold heated at 15 °C above the melting point of PCL (i.e. 60 °C) for 8 min at a pressure progressively increasing from 1 to 2 bars. A hydraulic press, heated platens and a temperature controller were employed. The mold and polymer were covered with Teflon<sup>®</sup> sheets in

order to avoid polymer adhesion to the heated plates. PCL films with a thickness close to 200  $\mu\text{m}$  were recovered after cooling the mold to room temperature.

CHX was incorporated by solvent casting. Specifically, 0.7 g of PCL and 3.5 mg of CHX (i.e. 0.5 w/w-%) were dissolved in 10 mL of an ethanol/chloroform 1:2 (v/v) mixture and the resulting solution was allowed to evaporate at room temperature. The obtained films were cut in small pieces and melt pressed as above explained. Smooth films with a similar thickness (i.e. 220  $\mu\text{m}$ ) were obtained.

### **Preparation of multilayered matrices**

Layers of PCL films and poly(GL)-*b*-poly(GL-*co*-TMC-*co*-CL)-*b*-poly(GL) electrospun mats were assembled alternately to obtain a five layer system, as shown in Figure 1b. Specifically, the two outer and the middle sheets corresponded to PCL films (i.e. film-mat-film-mat-film). These five layers placed in a mold of 1 cm x 2 cm x 0.5 cm internal dimensions were heated at 75 °C (i.e. 15 °C above the PCL melting point) for 15 min using heating plates and a temperature controller. A pressure of 1 ton was applied to the assembly after the heating process by hydraulic press. The mold and polymeric assembly were covered with Teflon<sup>®</sup> sheets in order to avoid polymer adhesion to the heated platens. After melt pressing the reinforced matrices were obtained. The molten PCL layers allowed to put together the different layers, leading to macroscopically homogeneous samples in which poly(GL)-*b*-poly(GL-*co*-TMC-*co*-CL)-*b*-poly(GL) electrospun fibers were embedded into the PCL matrix. The resulting matrices had a thickness close to 700  $\mu\text{m}$  and a PCL content close to 80 wt-%.

Different combinations of CHX loaded and unloaded layers, i.e. loading of CHX in one of the outer layers (PCL<sub>e</sub>), in the inner PCL layer (PCL<sub>i</sub>), in one electrospun mat (M(i)) and in the two electrospun mats (M(ii)), were evaluated. CHX load percentages were



close to 0.5 wt-%, 0.5 wt-%, 0.07 wt-% and 0.14 wt-% for PCL<sub>e</sub>, PCL<sub>i</sub>, M(i) and M(ii) systems, respectively.

### **Drug release**

Drug release experiments were performed with 1 cm × 1 cm square pieces (thickness close to 700 μm) representative of each drug loading configuration. These pieces were incubated at 37 °C in an orbital shaker at 80 rpm in tubes of 10 mL for 1 week. A 3:7 v/v mixture of PBS buffer and ethanol was used as the release medium. Additional experiments were also carried out in an ethanol medium and even in PBS when CHX was incorporated in the outer layer of PCL (PCL<sub>e</sub>). Samples were withdrawn from the release medium at predetermined time intervals and drug concentration was evaluated by UV spectroscopy using a Shimadzu 3600 spectrometer. Absorbance was measured at a wavelength of 260 nm. Calibration curves were prepared using different stock solutions of the assayed CHX drug in the different release media and relating the measured absorbance to concentration. The volume of the release medium was kept constant during the experiments by addition of fresh medium. All drug release tests were carried out using three replicates and the results were averaged.

Encapsulation efficiency was calculated by measuring the amount of drug incorporated into the scaffold by UV-vis absorbance measurements at a wavelength of 260 nm. Samples were dissolved in 0.5 mL of HFIP and subsequently the polymer was precipitated by addition of ethanol (0.5 mL). CHX was separated by centrifugation and dissolved in the solvent phase.

### **Antimicrobial test assays**

*E. coli* and *S. aureus* bacteria were selected to evaluate the antimicrobial activity of CHX loaded matrices. The bacteria were previously grown aerobically to exponential phase in broth culture (5 g/L yeast extract, 5 g/L NaCl, 10 g/L tryptone, pH 7.2).

Growth experiments were performed on a 24-well culture plate. All CHX loaded samples (1 cm x 1 cm and thickness close to 700  $\mu$ m) were placed into each well and an unloaded sample was used as a blank. Then, 2 mL of broth culture containing  $10^3$  CFU was added to the samples. Cultures were incubated at 37 °C and agitated at 80 rpm. Aliquots of 100  $\mu$ L were taken at predetermined time intervals for absorbance measurement at 650 nm in a microplate reader (every 2 h for 8 h, and after 12, 24 and 48 h from the starting time). Thus, turbidity was directly related to the relative bacterial growth by considering the maximum growth attained in the absence of any polymeric matrix (control).

Bacterial adhesion on matrices was also determined. Upon completion of growth experiments, culture media were aspirated and the material was washed three times with distilled water. Then, 0.5 mL of sterile 0.01 M sodium thiosulfate was added to each well to detach adhered bacteria. After 1 h agitation (100 rpm) at 37 °C, samples were removed and 1 mL of broth culture was added in each well. After filling the plate with fresh broth culture, the first sample was taken as a time 0 for adhesion assay. Then, plates were incubated at 37 °C and 100 rpm for 24 h. Bacterial number was determined as above indicated. All assays were conducted in quadruplicate and values were averaged.

In order to perform a qualitative evaluation, the pieces (1 cm  $\times$  1 cm  $\times$  700  $\mu$ m) of CHX loaded samples and an unloaded one, which was used as a blank, were placed into an agar diffusion plate and seeded separately with  $10^4$  CFU/mL of each bacterium. The culture medium was prepared with 18.5 g Brain Heart Infusion broth, 7.5 g Bacto™

Agar in 1 L of Milli-Q water and sterilized in an autoclave at 121 °C for 30 min. Plates were filled with 15 mL of medium and left to rest at room temperature to allow solidification of the medium. Inhibition halo images were taken after incubation of samples with bacteria at 37 °C for 24 h.

## **RESULTS AND DISCUSSION**

### **Electrospinning of unloaded and CHX loaded poly(GL)-*b*-poly(GL-*co*-TMC-*co*-CL)-*b*-poly(GL) nanofibers**

Low solubility of polymers having significant polyglycolide blocks limited the selection of an appropriate solvent for the electrospinning process to HFIP. A polymer concentration around 10 wt-% was found adequate to obtain nanofibers as previously described for polyglycolide (i.e. 8 wt-% in HFIP solution) [17]. Needle-collector distance had a limited influence on fiber morphology, and specifically distances between 12 and 15 cm allowed continuous and well-formed nanofibers to be obtained under most assay conditions. Lower values did not ensure complete solvent evaporation while, for longer distances, the population of narrower fibers increased.

The greatest difficulty in obtaining appropriate fiber morphology lay in the formation of a large proportion of irregular beads and even in the disruption of the electrospun nanofibers. Table 1 summarizes some representative experiments showing a beneficial effect at increased applied voltage and decreased flow rate. It is well known that the stretching process is enhanced at high voltages [20] whereas the decrease in the flow rate leads to small fiber diameters [21]. Solvents cannot be uniformly and completely evaporated at high flow rates, leading to the formation of abundant beads and even merging of fibers into a web [22]. The selected conditions (Table 1) corresponded to a voltage of 25 kV, a flow rate of 3.5 mL/h and a needle-collector distance of 12 cm

(Figures 2 and 3). Small variations led to defective morphologies, as shown in Figures 2a, 2b and 2c for higher flow rates and lower applied voltages.

SEM micrographs at different magnifications (Figures 3a, 3b and 3c) show that highly uniform and continuous nanofibers with smooth surfaces can be obtained under the selected processing conditions. Figure 4a plots a wide diameter distribution curve (i.e. from 200 to 900 nm) which follows a unimodal distribution. Most fibers have a diameter around 410 nm, with the average diameter being 500 nm and the standard deviation 118 nm.

The characteristics of the solution were drastically modified when the ionic CHX compound was added since, logically, the electrical conductivity of the **solution changed**. It is well established that an increase of solution conductivity tends to reduce fiber diameter because of the increase in electrical charge carried by the jet, and therefore in resulting tensile force, in the presence of an electric field [23]. Processing conditions were also modified (Table 1) in order to avoid fiber disruption and formation of droplets at low flow rates. In any case, continuous and homogeneous nanofibers (Figures 3d, 3e and 3f) could be obtained at 5 mL/h keeping both applied voltage (i.e. 25 kV) and needle-collector distance (i.e. 12 cm). High magnification SEM images (Figure 3e) revealed a smooth fiber surface, but also the presence of some very small crystals that could be attributed to CHX. They also showed the presence of two fiber populations, as could also be deduced from the diameter distribution in Figure 4b. The more abundant population corresponds to an average diameter of 150 nm and a standard deviation of 38 nm, whereas values of 320 nm and 90 nm characterize the **other** one. At any rate, the maximum diameter was close to 600 nm, a value significantly lower than that determined for unloaded fibers (i.e. 900 nm).

### **Preparation of multilayered PCL matrices containing poly(GL)-*b*-poly(GL-*co*-TMC-*co*-CL)-*b*-poly(GL) nanofibers**

The thermal molding process allowed nanofibers to be successfully integrated in the PCL matrix. In fact, only some edges of the molded pieces reveal the five-layered configuration, as shown in Figure 5a, probably because of deficient pressure on the borders of the mold. Nevertheless, comparison of Figures 5b and 5c demonstrates the ability of PCL to flow into electrospun scaffolds because of its moderate viscosity at the molding temperature and the porosity of scaffolds. Figure 5b illustrates the initial morphology, where a scaffold appears surrounded by two PCL films whereas Figure 5c shows how the different layers cannot be distinguished in the inner sections of the piece after completion of the molding process. The presence of fibers relatively well distributed in the matrix can be envisaged in high magnification images (see arrows in the inset of Figure 5c). It is worth noting that the fracture surfaces of molded pieces obtained after cracking them in liquid nitrogen had a homogeneous appearance similar to that observed for the initial PCL films (see inset in Figure 5c).

NMR spectra (Figure 6a) allowed the final composition of multilayer matrices and, specifically, the weight percentages of PCL and the segmented copolymer to be determined. The last gave rise to a complex spectrum due to the sequence sensitivity of the different units (i.e. glycolic acid,  $\epsilon$ -caprolactone and trimethylene carbonate), which had well-differentiated signals associated with the different types of glycolic acid protons in the 4.9-4.5 ppm range and minor signals associated with trimethylene carbonate and  $\epsilon$ -caprolactone units. The spectrum of multilayer samples showed predominant peaks associated with PCL and, specifically, a clear triplet at 2.24 ppm that corresponds to the CH<sub>2</sub>CO protons. The weight percentage of the segmented copolymer (Cop-%) was determined with equation 1 taking into account the areas of representative

peaks (i.e.  $A_{4.9-4.5}$  and  $A_{2.3-2.2}$  for glycolyl and  $\epsilon$ -caproyl units, respectively), the molecular weights of glycolyl (i.e. 58 g/mol) and  $\epsilon$ -caproyl units (114 g/mol), and finally the weight percentages of glycolyl (72%) and  $\epsilon$ -caproyl (14%) residues in the segmented copolymer.

$$\text{Cop-\%} = (A_{4.9-4.5} \times 58) / [(A_{4.9-4.5} \times 58) + (A_{2.3-2.2} - (A_{4.9-4.5} \times 58 \times 0.14 / 0.72))] \times 100 \quad (1)$$

Composition was analyzed by sampling the diagonal of the molded pieces at four equidistant points. Results revealed a highly homogeneous composition (i.e. Cop-% varied between 18 and 22 %) that was in full agreement with the theoretical value (20 %) deduced from the weight of PCL films (ca. 48 mg) and scaffolds (ca. 12 mg) introduced in the mold. That is, losses caused by the flow of molten PCL were negligible.

The FTIR spectrum of the multilayer matrix (Figure 6b) showed predominant PCL bands, although those corresponding to PGL could also be distinguished. Bands at 1414, 972 and 902  $\text{cm}^{-1}$  are significant because they are assigned to the crystalline phase of PGL [24], with the two first peaks being clearly detected in the multilayer matrix. Spectra of loaded matrices were similar due to the complexity of the FTIR spectra and the small amount of incorporated drug.

### **Thermal properties of multilayered PCL matrices containing poly(GL)-*b*-poly(GL-*co*-TMC-*co*-CL)-*b*-poly(GL) nanofibers**

DSC heating scans of electrospun scaffolds (Figure 7) revealed that the segmented copolymer was able to crystallize during the electrospinning process. The first heating scan was characterized by a very complex melting peak indicative of the existence of crystalline lamellae with different thicknesses. The first peak appeared around 170 °C whereas the last and most intense one was observed around 193 °C. The intensity ratio

between peaks varied depending on the region of the scaffold and, specially, between samples processed in different batches. Note, for example, the different relative intensity of the peak at 170 °C in the inset of Figure 7a. The high melting temperatures are associated with the fusion of polyglycolide hard segments (i.e. 229 °C is the reported equilibrium melting temperature of polyglycolide [24]) and its enthalpy allowed the crystallinity of the sample to be estimated considering a value of 11.8 kJ/mol for a 100% crystalline polyglycolide [25]. Crystallinities of 22% and 21% were thus determined for the as processed scaffold and the melt crystallized sample (Figure 7b), respectively. These crystallinities increased to 39% and 37% when were referred to the hard segment content (i.e. the melting enthalpy was recalculated taking into account the weight percentage of polyglycolide hard segments in the copolymer). The DSC heating scan of melt crystallized samples basically corresponded to the melting of thick lamellae since only a peak at 192 °C was detected. On the other hand, once again a very broad melting peak indicative of the presence of lamellae with different thicknesses was observed for samples quenched from the melt state. Nevertheless, no well-defined low temperature peak could be distinguished in this case. Melting enthalpies of melt crystallized (i.e. cooled from the melt at a rate of 10 °C/min) and quenched samples (i.e. cooled from the melt at the maximum rate allowed by the equipment) were highly similar, as can be deduced from the heating traces in Figures 7c and 7d. Associated enthalpies were high and indicative of the great ability of the segmented copolymer to crystallize. Calculated crystallinities (i.e. 21% and 20%) were slightly lower than those determined for the electrospun samples, showing that crystallization was easier when polymer chains were oriented by the electrospinning process despite the reduced time involved in the evaporation of the solvent. The heating scan of the melt quenched

sample showed a single glass transition temperature at 3 °C, which indicates a miscible amorphous phase constituted by soft and non-crystallized hard segments.

For the sake of completeness, the DSC trace of the final CHX loaded multilayer matrix is shown in Figure 7e. In this case, melting peaks associated with the fusion of PCL (melting peak at 57 °C) and PGL can be distinguished, and thus crystallinities of 64% (16.2 kJ/mol was considered as the melting enthalpy for 100% crystalline PCL [26]) and 82% were obtained for the PCL and PGL crystalline phases, respectively. These percentages were determined considering the content of PCL and PGL hard blocks in the scaffold. Note that the crystallinity of the PGL phase was clearly enhanced by a thermal annealing process during molding. Logically, PGL had a complex fusion, with peaks at 171 °C and 193 °C. In this case, the predominant peak was 171 °C, suggesting that thinner lamellae were stabilized during the annealing process, thus hindering recrystallization/reordering into thicker lamellae during heating. Finally, the heating run of a melt-crystallized sample (Figure 7f) showed that only the population of the thickest PGL lamellae was produced during crystallization as only the peak at 193 °C was observed. The incorporated CHX drug did not have a remarkable influence on thermal behavior because DSC traces could not be distinguished from those obtained of unloaded samples (not shown).

TG and DTG curves (Figure 8) showed the high thermal stability of the multilayer matrices, which had an onset degradation temperature of 250 °C and decomposed according to two steps with DTG peak temperatures at 350 °C and 410 °C. These degradation processes were in full agreement with those observed for the nanofibrous scaffold (i.e. single peak at 350 °C) and the PCL film (i.e. single peak at 410 °C), with the weight loss associated with the first step being smaller due to the lower content of nanofibers (i.e. 19 wt-%) in the matrix.



It is clear that the multilayer sample could be prepared without any evidence of thermal degradation because nanofibers were obtained by electrospinning at room temperature and the molding process was performed at a temperature different from that at the beginning of decomposition due to the low melting temperature of PCL. However, TG and DTG curves of CHX showed a relatively low stability that could affect the processing of multilayer matrices. Specifically, CHX had a complex three step degradation process with an onset degradation temperature of 175 °C and DTG peak temperatures of 250 °C, 355 °C and 466 °C. Incorporation of CHX in the electrospun scaffold had a remarkable influence on its onset degradation temperature, which decreased to 200 °C despite the low amount of loaded drug (ca. 0.5 wt-%). Furthermore, the temperature of the first DTG peak decreased from 355 °C to 330 °C. In addition, a char yield close to 4% was detected in the corresponding DTG curve, in agreement with the high residue observed in the degradation of the CHX drug caused by its high aromatic content. Although **in this case processing** was not problematic due to the low temperature range, the thermogravimetric result is interesting because it points out that caution should be taken when other polymers with a higher melting point (e.g. polylactide) are selected as matrices.

### **Mechanical properties of multilayered PCL matrices containing poly(GL)-*b*-poly(GL-*co*-TMC-*co*-CL)-*b*-poly(GL) nanofibers**

Representative stress-strain curves of the different fabrics are shown in Figure 9. Several points deserve attention:

- a) Unloaded scaffolds have low Young's modulus (i.e. 20 MPa), as expected for an electrospun sample. **This modulus is limited due to slippage between nonwoven fibers. Final deformation and maximum stress become close to 170% and 2 MPa, respectively. The latter value clearly increased (i.e. 5 MPa) when the scaffold was loaded with CHX**

while modulus and final strain remained similar. The differences observed in fiber morphology (e.g. a significant reduction in diameter) were due to the incorporation of CHX.

b) PCL films showed a typical behavior characterized by high elastic modulus (i.e. 180 MPa) due to high crystallinity of PCL, maximum stress of 9 MPa at the necking point and a plastic region that extends to a final deformation higher than 200% (i.e. 600% not shown). These properties changed drastically when CHX was incorporated even for a low percentage such as 0.5 wt-%. Thus, maximum stress decreased to 7 MPa and deformation to 20%. Crystallization was also slightly hindered, and consequently modulus decreased to 165 MPa.

c) The unloaded multilayer matrix had slightly higher Young's modulus than the PCL film (i.e. from 180 MPa to 220 MPa) due to the incorporation of nanofibers. In addition, an increase in maximum stress (i.e. 17 MPa) indicative of a reinforcing effect, and therefore of the existence of relatively good interactions between the matrix and the nanofibers, was observed. Elongation at break (i.e. 55%) was lower than that of the matrix due to the stiff nature of the added fibers. It should be emphasized that multilayer matrices having CHX loaded in the nanofibers showed clearly improved properties (235 MPa, 23 MPa and 55% for Young's modulus, maximum stress and final deformation, respectively) since the nanofiber diameters decreased, as above indicated. The most important conclusion is that these loaded multilayer samples displayed significantly better properties than PCL films having similar drug loading.

### **CHX release from multilayer matrices**

Release behavior was first studied in ethanol medium because it has a great ability to swell the polymer matrix and favor drug delivery. Furthermore, ethanol is also a good

solvent of CHX. That is why results about the use of ethanol appear useful to highlight the ability of the different layers to retain the drug, if that is the case.

Figure 10a shows almost immediate release for the drug loaded in the outer PCL layer, with complete delivery being achieved after only 30 h of exposure. Release was also fast for the drug loaded the inner PCL layer, although in this case more than 100 h was required to obtain a relative release percentage of 98%. Basically, the difference in the release of CHX loaded in the outer and the inner PCL films is due to the variation of the diffusion path of the drug.

In contrast, a significantly different behavior was observed when the drug was incorporated into the scaffolds. Logically, increased retention could not just be due to an increased diffusion path. Therefore, it should be considered that CHX can establish better interactions with the hydrophilic PGL rich copolymer than with the hydrophobic PCL. Interestingly, Figure 10 also shows that different release profiles were attained depending on whether the drug was incorporated in one or both scaffolds. Thus, in the first case, release was 90% after 100 h of exposure while in the second case it was only 80% after the same period. The increased amount of loaded nanofibers clearly hindered drug release since it had more chance to interact with them. Note that an opposite result should be expected because of the higher drug concentration inside the matrix when both scaffolds were loaded.

Delivery of CHX into aqueous PBS medium was insignificant, even when the drug was loaded in the outer PCL layer (i.e. 15% after 100 h) (Figure 10b, solid line). It is clear that water was unable to swell the hydrophobic polymer properly, and thus facilitate drug diffusion. Differences with the other loaded matrices were, logically, irrelevant. Figure 10b also illustrates that the release behavior in function of the ethanol/water ratio. Specifically, the system with CHX in both scaffold layers shows the highest

sensitivity for a decrease of the ethanol content from 100% to 70%. Note, for example, that the release percentage for the M(ii) configuration decreased from 80% to 70% after 100 h of exposure. This difference in behavior can also be evaluated quantitatively through the decrease in the release constant from  $0.10 \text{ h}^{-0.5}$  to  $0.08 \text{ h}^{-0.5}$  when a typical Higuchi equation is applied:<sup>[27,28]</sup>

$$M_t/M_0 = k_H t^{(1/2)}, \quad (2)$$

where  $k_H$  is the Higuchi release constant,  $M_t$  is the percentage of drug released at time  $t$ , and  $M_0$  is the maximum percentage of released drug.

### **Antibacterial properties of CHX loaded matrices**

The antimicrobial effect of CHX loaded matrices was evaluated quantitatively by considering the growth curves of Gram-negative (*E. coli*) and Gram-positive (*S. aureus*) bacteria, (Figures 11a and 11b). Clearly, the unloaded matrix is highly susceptible to bacterial infection, with a latency phase that extends over a period of 4 h and followed by an exponential growth (log) phase. A significant decrease in bacterial proliferation was only detected when CHX was loaded in the outer PCL film. Nevertheless, the growth curve was again characterized by similar latency and exponential growth phases. Results indicate that an immediate bacteriostatic effect was attained by incorporating the drug in the outer layers. However, the possibility of having a drug reservoir for long term events is also interesting. In this sense, it is clear that loading of CHX in the inner electrospun scaffolds led to greater drug release after 2000 min (i.e. after the drug from PCL was completely delivered). Interestingly, growth inhibition during the period of 8 to 24 h was slightly higher for the M(ii) multilayer matrix than for the unloaded blank and even for the PCL sample (note the decrease in the slope of the *S. aureus* growth curves). In fact, bacterial adhesion tests (Figure 12) reveal that PCL was the only

loaded matrix with a clear bacteriostatic effect for long term assay (24 h) and that *S. aureus* was more sensitive to CHX than *E. coli*. Thus, adhesion was 90 % and 85 % with respect to the control for *E. coli* and *S. aureus*, respectively. The bactericidal effect was also evaluated qualitatively by agar tests, i.e. measuring the inhibition halos around the multilayer fabrics. This method is highly problematic to evaluate the bactericidal effect of hydrophilic drugs such as CHX since their release in the hydrophobic agar medium is difficult. Results (Figure 13) point out that inhibition halos were only significant for PCLe samples, regardless of the type of bacteria, and show a clear bactericidal activity due to the unfavorable test medium that had been expressly chosen. Logically, samples loaded in the nanofibers did not show bactericidal activity in these short time events.

## CONCLUSIONS

Segmented copolymers having 57 wt-% of polyglycolide hard segments and soft segments constituted by glycolide, trimethylene carbonate and  $\epsilon$ -caprolactone units can be successfully electrospun from HFIP diluted solutions. Continuous and uniform nanofibers with an average diameter of 500 nm and a smooth texture were attained using voltage, flow rate and needle-collector distance of 25 kV, 3.5 mL/h and 12 cm, respectively. Increase of flow rate and decrease of voltage had a strong effect on fiber morphology. Specifically, bead formation was clearly enhanced.

Electrospinning allowed fibers loaded with a bactericidal drug, i.e. chlorhexidine, to be obtained, although processing parameters had to be modified because of the increase in electrical conductivity of the solution. A bimodal diameter distribution was achieved, with 150 and 320 nm being the mean diameters of the two populations.

Electrospun nanofibers were highly crystalline, as revealed by FTIR and DSC measurements. Incorporation of CHX had little influence on crystallinity because the expected negative effect could be compensated by the higher polymer orientation attained in the stretched nanofibers.

Molding of a five layer assembly of alternate PCL films and electrospun scaffolds based on a PGL rich copolymer gave rise to a PCL matrix reinforced with well distributed nanofibers. Favorable interactions were probably established between the matrix and the soft segments containing  $\epsilon$ -caprolactone. Enhancement of mechanical properties of loaded multilayer matrices proved that the presence of nanofibers could compensate for the decrease in mechanical performance of PCL layers loaded with CHX.

Drug release experiments revealed that the multilayer system was able to ensure fast release of CHX loaded in the outer PCL layers while delayed delivery was achieved for CHX loaded in the nanofibers due to the good interactions established between the drug and the hydrophilic polyglycolide component. This tunable release behavior appears highly interesting to obtain a short and long term bactericidal effect, as demonstrated by growth inhibition and cell adhesion experiments.

**Acknowledgements.** Authors are in debt to supports from MINECO and FEDER (MAT2015-69547-R) and the Generalitat de Catalunya (2014SGR188). The work has also been carried out under a research agreement between B. Braun Surgical, S. A. and the Universitat Politècnica de Catalunya. Ms Y. Márquez thanks financial support from B. BRAUN Surgical S.A.

## REFERENCES

- [1] M. M. Bergshoef, G. J. Vancso, *Adv. Mater. (Weinheim, Ger.)* **1999**, *11*, 1362.
- [2] H. Fong, *Polymer* **2004**, *45*, 2427.
- [3] E. D. Pinho, A. Martins, J. V. Araújo, R. L. Reis, N. M. Neves, *Acta Biomater.* **2009**, *5*, 1104.
- [4] L. J. del Valle, A. Díaz, M. Royo, A. Rodríguez-Galán, J. Puiggalí, *eXPRESS Polym. Lett.* **2012**, *6*, 266.
- [5] K. Molnár, E. Kostáková, L. Mészáros, *eXPRESS Polym. Lett.* **2014**, *8*, 62.
- [6] L. J. del Valle, R. Camps, A. Díaz, L. Franco, A. Rodríguez-Galán, J. Puiggalí, *J. Polym. Res.* **2011**, *18*, 1903.
- [7] E. Díaz-Celorio, L. Franco, A. Rodríguez-Galán, J. Puiggalí, *Eur. Polym. J.* **2012**, *48*, 60.
- [8] V. J. Mkhabela, S. S. Ray, *J. Nanosci. Nanotechnol.* **2014**, *14*, 535.
- [9] T. K. Dash, V. B. Konkimalla, *J. Controlled Release* **2012**, *158*, 15.
- [10] Y. Ikada, H. Tsuji, *Macromol. Rapid Commun.* **2000**, *3*, 21.
- [11] S. S. Spearman, I. V. Rivero, N. Abidi, *J. Appl. Polym. Sci.* **2014**, *131*, 40224.
- [12] Y. Márquez, L. Franco, J. C. Martínez, F. Estrany, P. Turon, J. Puiggalí, *Eur. Polym. J.* **2015**, *73*, 222.
- [13] Y. Márquez, J. C. Martínez, P. Turon, L. Franco, J. Puiggalí, *Fibers* **2015**, *3*, 348.
- [14] Y. Márquez, L. Franco, P. Turon, J. Puiggalí, *Thermochim. Acta* **2014**, *585*, 71.
- [15] Y. Márquez, L. Franco, P. Turon, J. Puiggalí, *Polym. Degrad. Stab.* **2014**, *98*, 2709.
- [16] S. Oberhoffner, H. Planck, *EP 0835895* **1996**.

- [17] Y. You, B. M. Min, S. J. Lee, T. S. Lee, W. H. Park, *J. Appl. Polym. Sci.* **2004**, *95*, 193.
- [18] J. B. Leikin, F. P. Paloucek, *Poisoning and Toxicology Handbook* **2008**, 183.
- [19] J. B. D. Green, T. Fulghum, M. A. Nordhaus, *Science against Microbial Pathogens: Communicating Current Research and Technological Advances*, Formatex Microbiology Books Series, **2011**.
- [20] S. Shenoy, W. Bates, H. Frisch, G. Wnek, *Polymer* **2005**, *46*, 3372.
- [21] X. Zong; K. Kim; D. Fang; S. Ran, B. S. Hsiao, B. Chu, *Polymer* **2002**, *43*, 44032.
- [22] X. Yuan; Y. Zhang; C. Dong; J. Sheng; *Polym. Int.* **2004**, *53*; 1704.
- [23] C. J. Angamma, S. H. Jayaram, *IEEE Trans. Ind. Appl.* **2011**, *47*, 1109.
- [24] G. Kister, G. Cassanas, M. Vert, *Spectrochim. Acta, Part A* **1997**, *53*, 1399.
- [25] B. V. Lebedev, A. A. Yepstropov, V. G. Kiparisova, V. I. Belov, *Polym. Sci. U.S.S.R.* **1978**, *20*, 32.
- [26] B. Wunderlich, *Macromolecular physics*, Academic Press **1980**, 3.
- [27] T. Higuchi, *J. Pharm. Sci.* **1963**, *52*, 1145.
- [28] R. W. Baker, *Controlled Release of Biologically Active Agent*, John Wiley & Sons **1987**.



## FIGURE CAPTIONS

**Figure 1.** a) Chemical structures of poly(GL)-*b*-poly(GL-*co*-TMC-*co*-CL)-*b*-poly(GL) (Monosyn<sup>TM</sup>), poly( $\epsilon$ -caprolactone) and the selected CHX hydrophilic drug. b) Schematic representation showing the distribution of layers and the different CHX loading configurations.

**Figure 2.** Optical micrographs showing the improvement of fiber morphology by decreasing flow rate and increasing applied voltage. A considerable number of beads were observed at 5 mL/h and 12.5 kV (a), which contrasts with the number of uniform fibers obtained at 3.5 mL/h and 25 kV (d). For the sake of completeness, fibers obtained under intermediate conditions are also shown; 5 mL/h and 15 kV (b) and 3.5 mL/h and 15 kV (c).

**Figure 3.** SEM micrographs showing unloaded (a,b,c) and CHX loaded (d,e,f) poly(GL)-*b*-poly(GL-*co*-TMC-*co*-CL)-*b*-poly(GL) electrospun nanofibers at different magnifications. Nanofibers were obtained under optimized conditions.

**Figure 4.** Diameter distribution curves of unloaded (a) and CHX loaded (b) poly(GL)-*b*-poly(GL-*co*-TMC-*co*-CL)-*b*-poly(GL) electrospun nanofibers obtained under optimized conditions.

**Figure 5.** SEM micrographs showing the lateral edge of the final multilayer matrix (a), the assembly of an electrospun mat between two PCL films before the melt pressing process (b) and a lateral view of the inner part of the matrix after being cracked in liquid nitrogen (c). The insets show a magnification where nanofibers can be distinguished as it is pointed by the red arrows and a section of the initial PCL film.

**Figure 6.** a) NMR spectrum of a multilayer matrix with assignment of main peaks. b) FTIR spectrum showing characteristic bands of PCL and poly(GL)-*b*-poly(GL-*co*-TMC-*co*-CL)-*b*-poly(GL) polymers. Blue arrows point out the characteristic PGL bands associated with the crystalline phase that can be detected in the electrospun scaffold.

**Figure 7.** DSC heating (a), cooling (b) and subsequent heating (c) scans of poly(GL)-*b*-poly(GL-*co*-TMC-*co*-CL)-*b*-poly(GL) electrospun nanofibers. The inset of a) shows the melting peak observed for another scaffold processed under the same conditions. d) Heating scan of a melt quenched electrospun sample. e) Heating scan of a CHX loaded multilayer piece. f) Heating scan of a CHX loaded multilayer piece after crystallizing from the melt state.

**Figure 8.** TGA (a) and DTGA (b) curves for the indicated representative samples.

**Figure 9.** Stress-strain curves of poly(GL)-*b*-poly(GL-*co*-TMC-*co*-CL)-*b*-poly(GL) electrospun mats (green lines), PCL films (red lines) and multilayer matrices (orange lines). Unloaded and CHX loaded samples are represented by dashed and solid lines, respectively.

**Figure 10.** CHX release percentages in EtOH (a) and PBS-EtOH 30:70 (b) media for the different loading configurations of the multilayer matrix. For the sake of completeness, data in PBS medium are also plotted (solid line) for the configuration where CHX is loaded in the outer PCL films (PCL<sub>e</sub>).

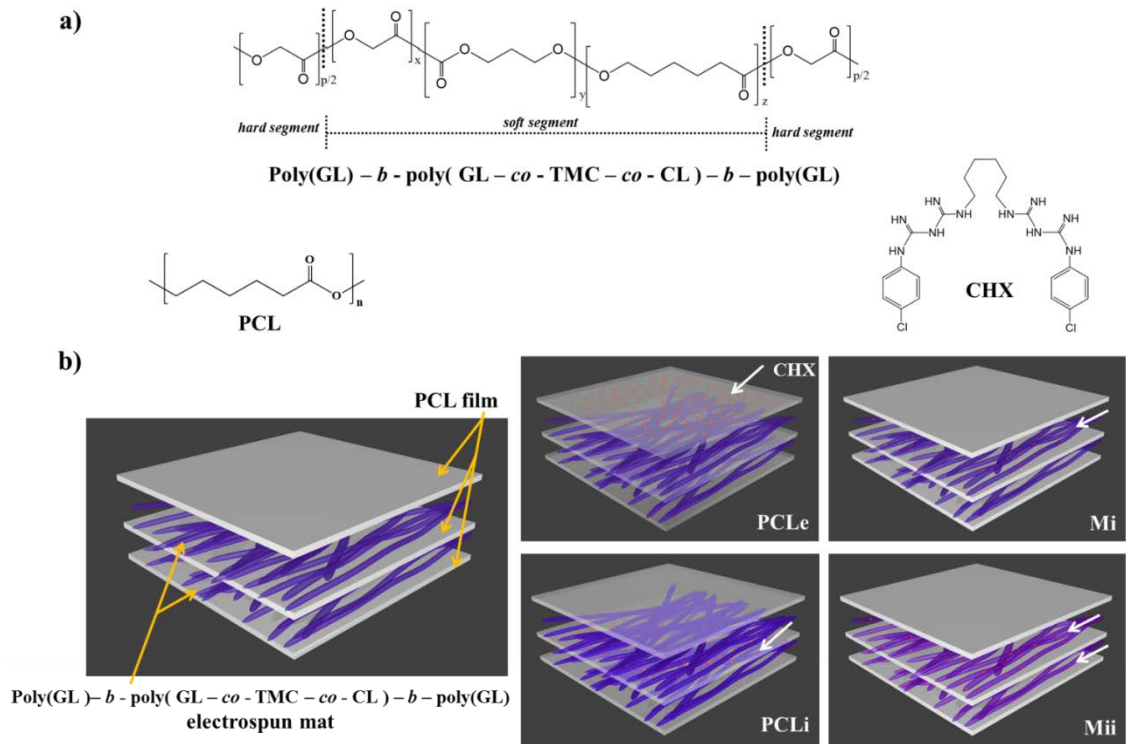
**Figure 11.** Growth curves of *E. coli* (a) and *S. aureus* (b) in the CHX loaded multilayer matrices and the unloaded one used as a blank.

**Figure 12.** Adhesion of *E. coli* (gray bars) and *S. aureus* (grid bars) on the CHX loaded multilayer matrices. Data concerning the culture plate as positive control and the unloaded matrix as blank are also provided.

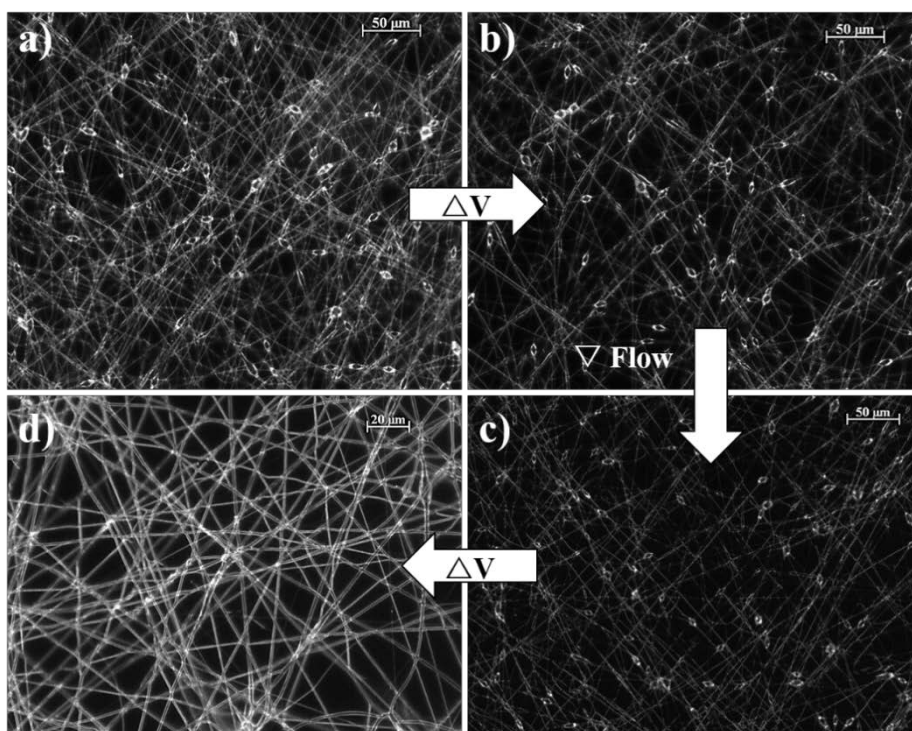
**Figure 13.** Images showing inhibition halos on agar plates seeded with *E. coli* and *S. aureus* caused by multilayer matrices **with loaded outer PCL film** and the electrospun mat. Images of blanks (unloaded matrices) are also provided.

**Table 1.** Morphology of unloaded and CHX loaded electrospun poly(GL)-*b*-poly(GL-*co*-TMC-*co*-CL)-*b*-poly(GL) samples induced depending on processing parameters (voltage, flow rate and needle-collector distance) .

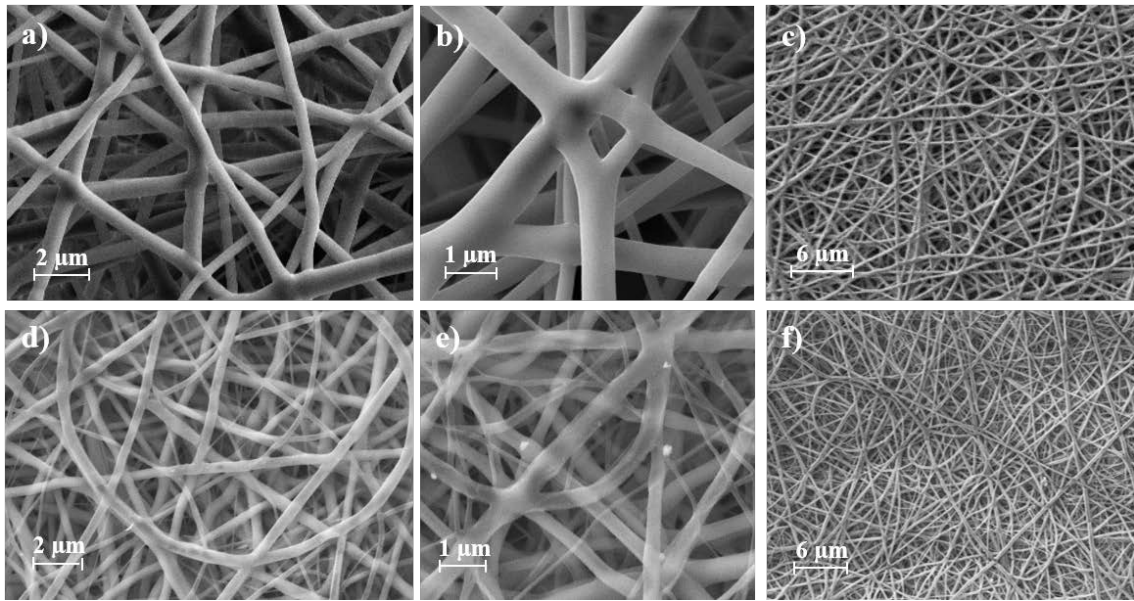
Assay	Voltage (kV)	Flow (mL·h <sup>-1</sup> )	Distance (cm)	Results
<b>Electrospun fibers</b>				
1	12.5	5	12.5	Many beads
2	15	5	15	Some beads
3	15	8	15	Some beads
4	15	3.5	12	Few beads
5	20	3.5	12	Few beads
<b>6</b>	<b>25</b>	<b>3.5</b>	<b>12</b>	<b>No beads</b>
<b>Electrospun fibers with CHX</b>				
1	25	3.5	12	Many beads
2	20	3.5	12	More beads. Disruption on fiber
3	20	7	12	Less beads but many fibers with oval droplet-like shape
4	20	5	12	Many beads
<b>5</b>	<b>25</b>	<b>5</b>	<b>12</b>	<b>No beads and only few oval droplet-like shape fibers</b>



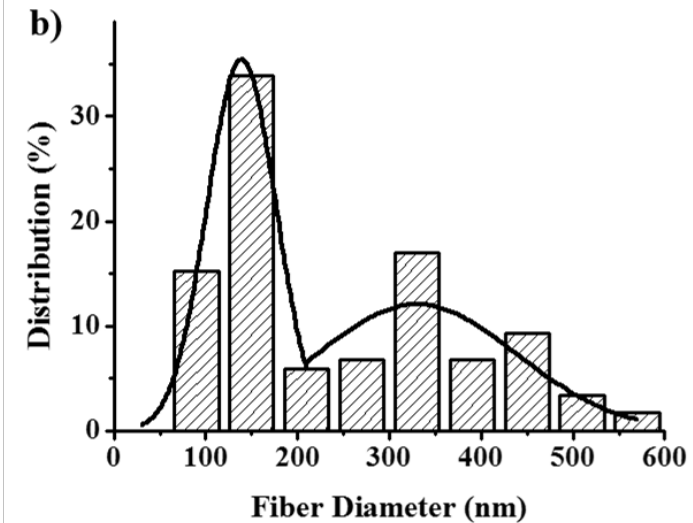
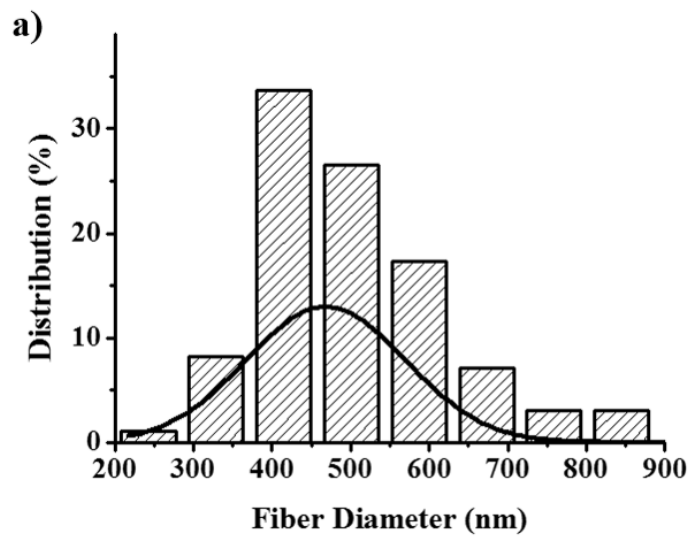
**Figure 1**  
**Márquez *et al.***



**Figure 2**  
*Márquez et al.*

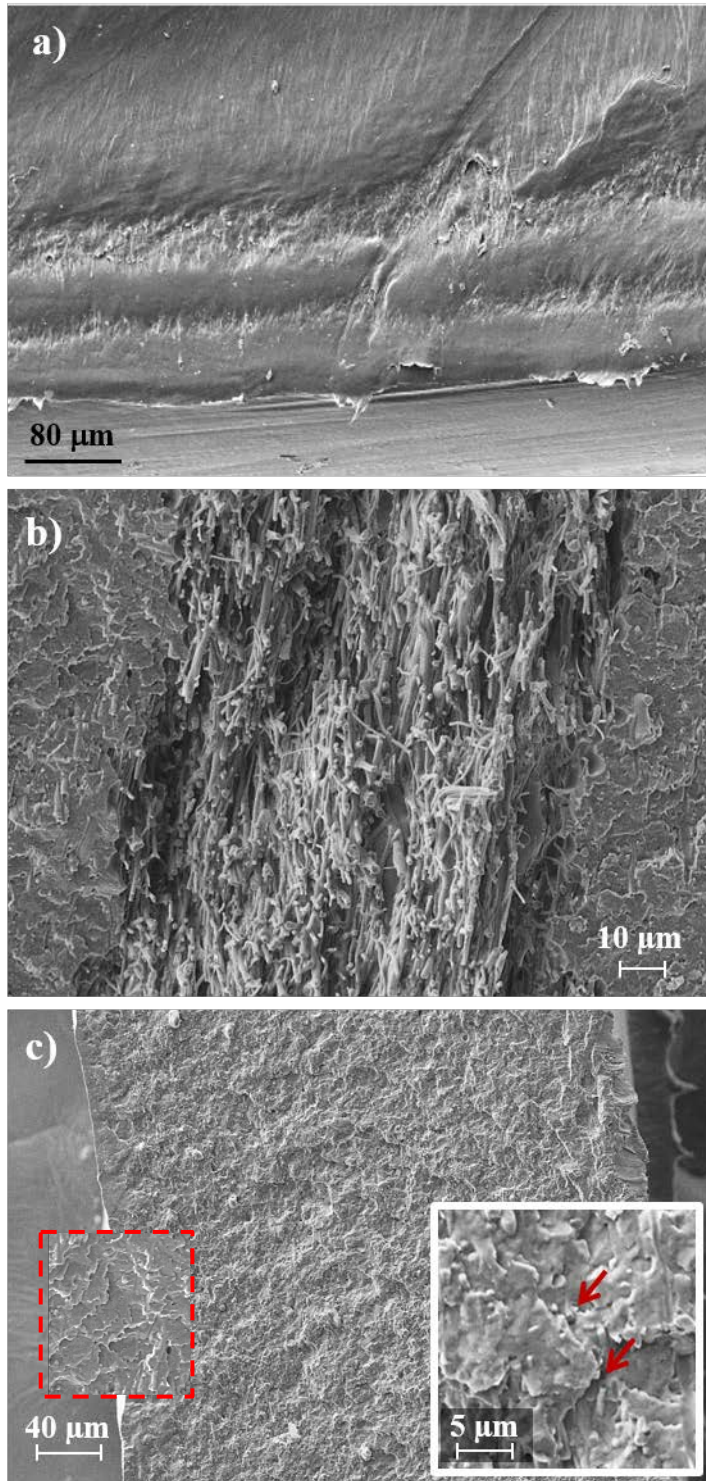


**Figure 3**  
*Márquez et al.*

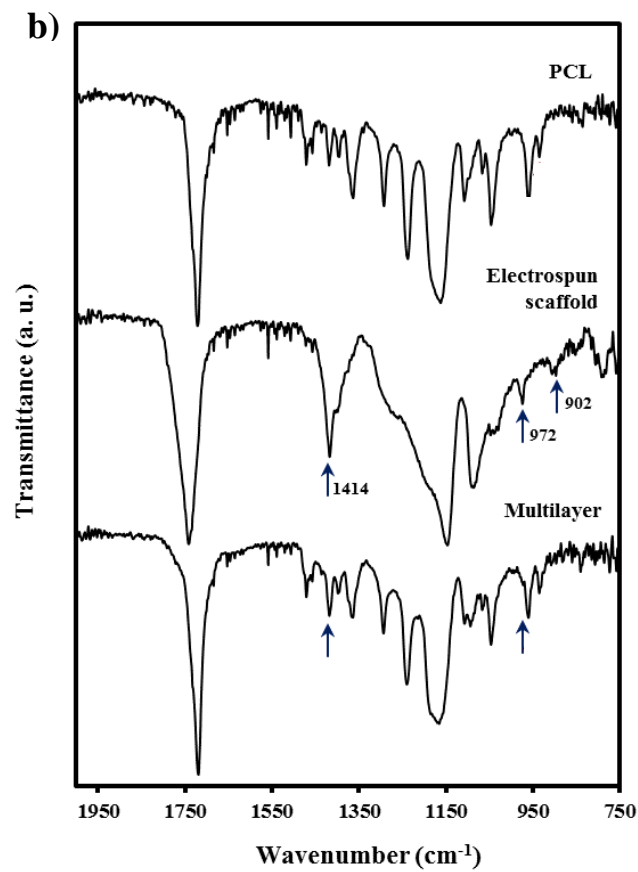
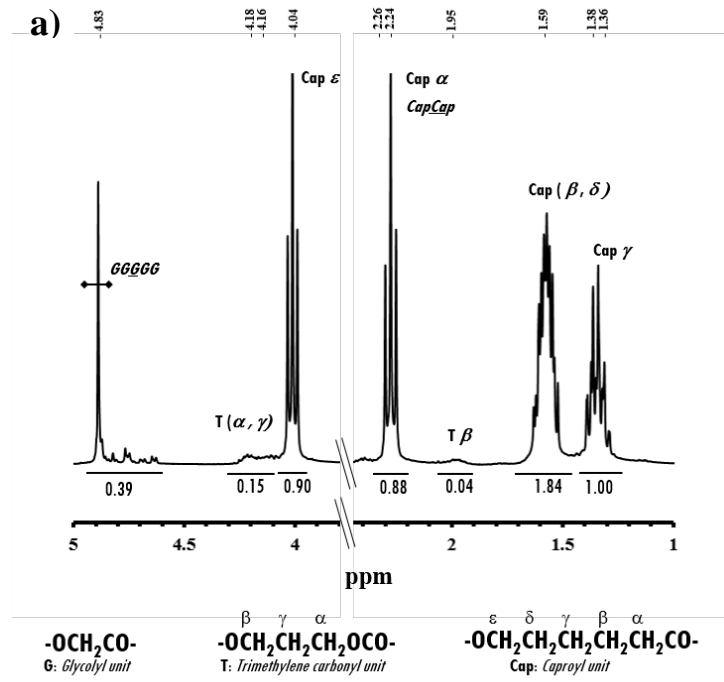


**Figure 4**  
*Márquez et al.*

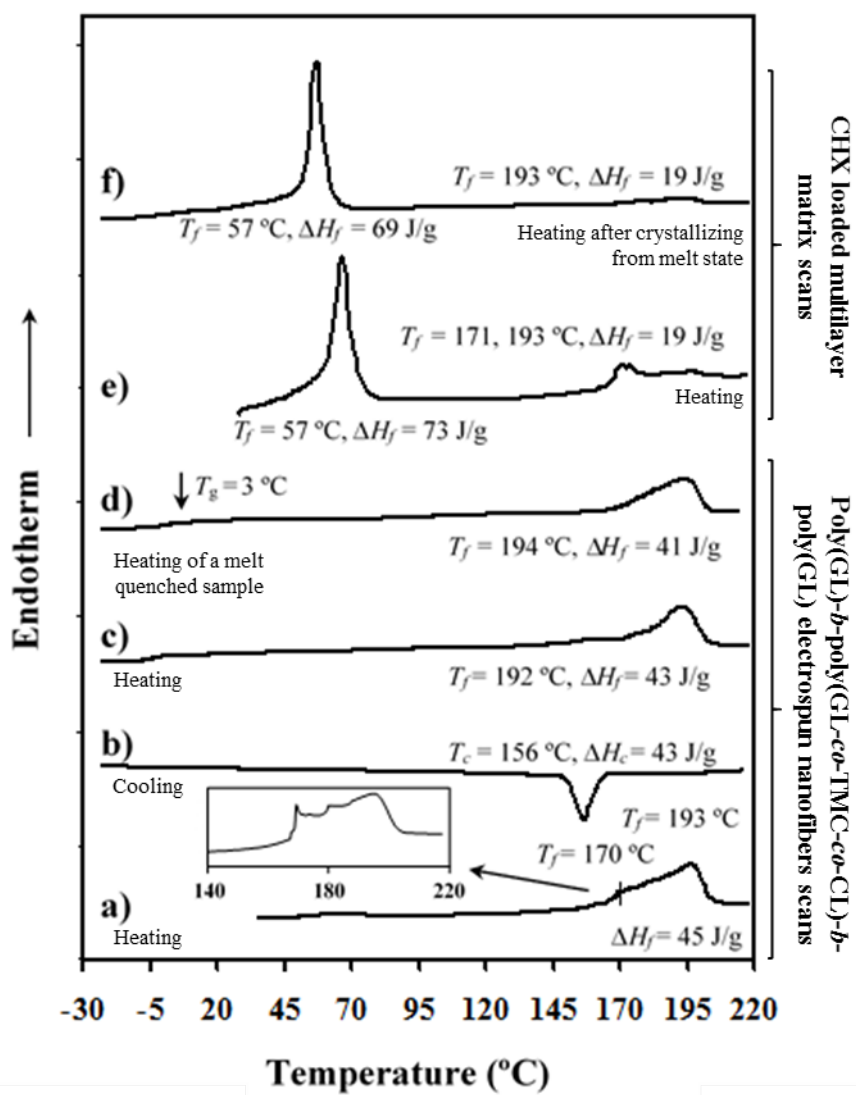




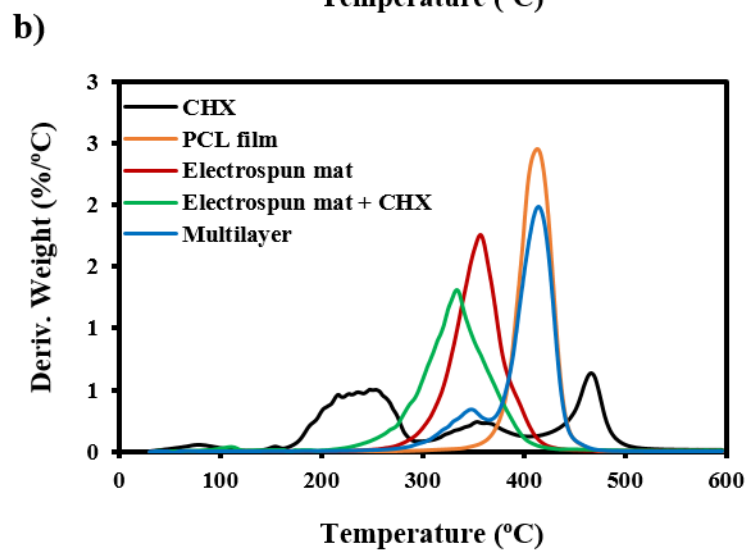
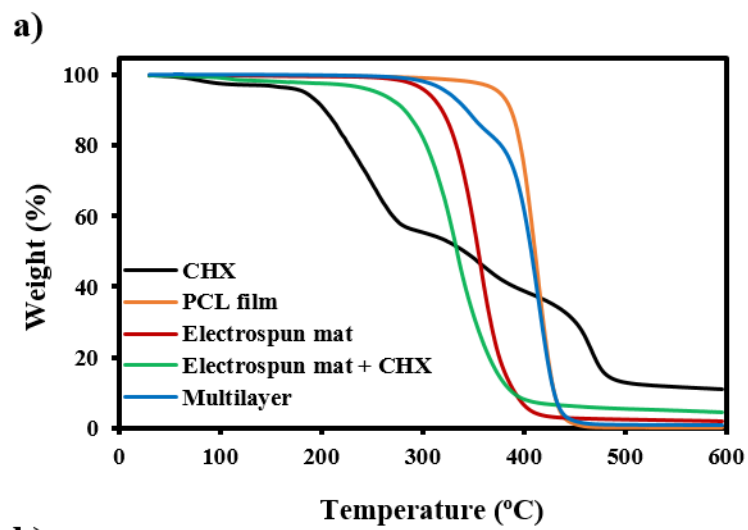
**Figure 5**  
*Márquez et al.*



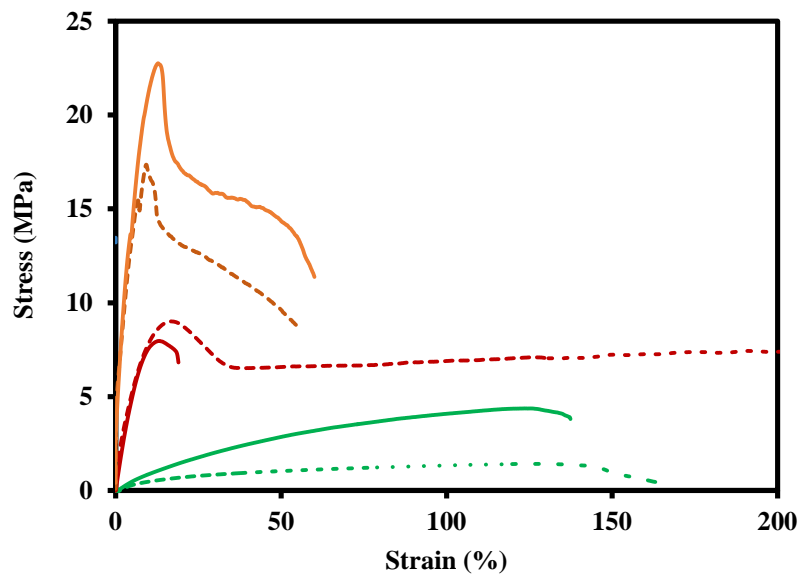
**Figure 6**  
Márquez *et al.*



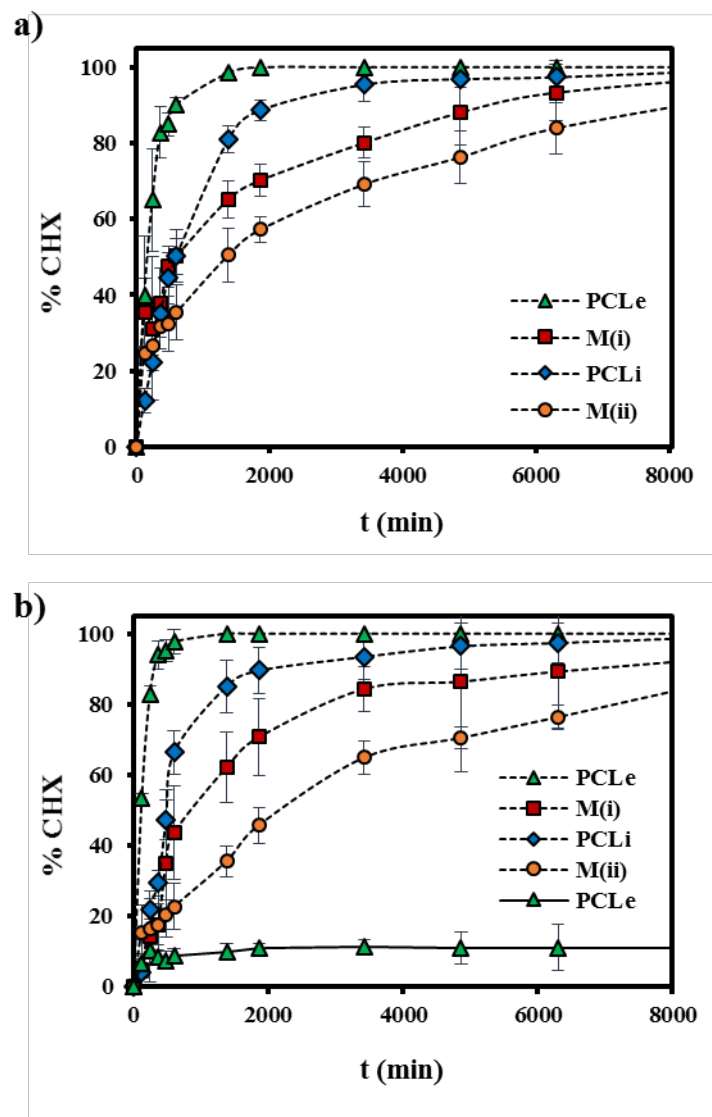
**Figure 7**  
**Márquez et al.**



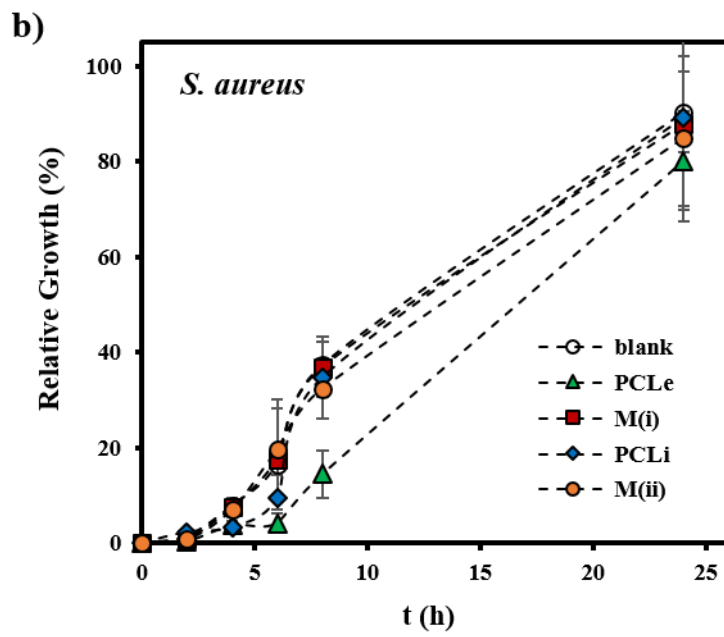
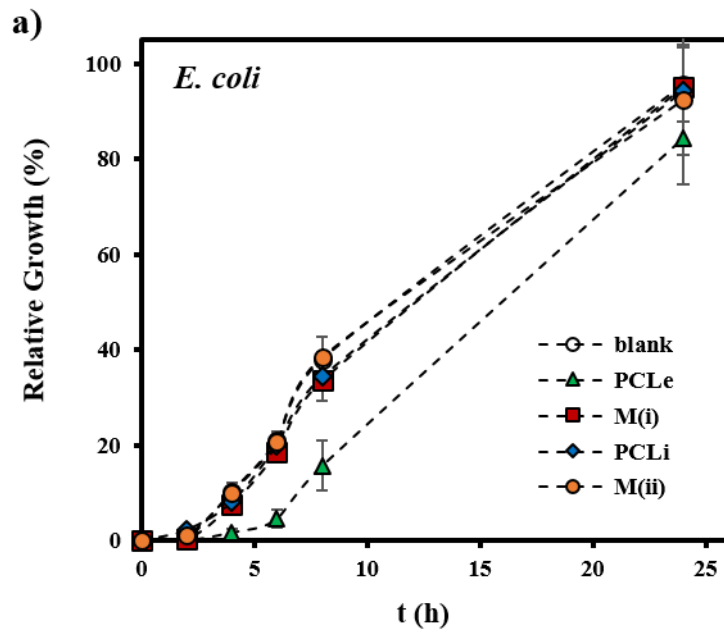
**Figure 8**  
*Márquez et al.*



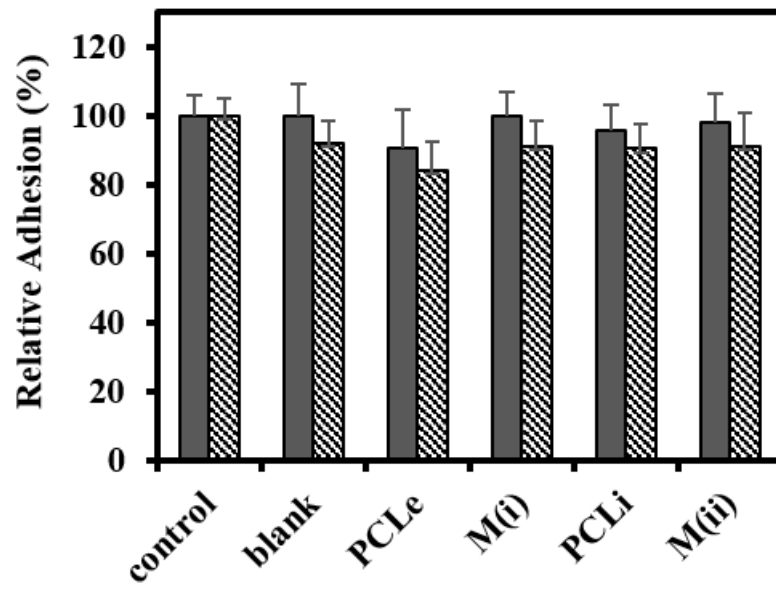
**Figure 9**  
**Márquez *et al.***



**Figure 10**  
Márquez *et al.*


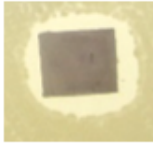






**Figure 11**  
Márquez *et al.*



**Figure 12**  
*Márquez et al.*



	blank	PCLe	M(i)
<i>E. coli</i>			
<i>S. aureus</i>			

**Figure 13**  
*Márquez et al.*

## Table of Contents

**Poly( $\epsilon$ -caprolactone) matrices reinforced with well distributed nanofibers of a polyglycolide rich copolymer are easily prepared by molding multilayered assemblies of alternate PCL films and electrospun scaffolds.** Drugs are loaded in specific layers giving rise to a tunable release. Short and long term bactericidal effects are interestingly derived as demonstrated by growth inhibition and cell adhesion experiments.

Y. Márquez, L. Franco, P. Turon, L. J. del Valle, J. Puiggali\*

Tunable Drug Loading and Reinforcement of Polycaprolactone Films by Means of Electrospun Nanofibers of Glycolide Segmented Copolymers

